

## Article

# Mineralogical Characterization of Early Bronze Age Pottery from the Svilengrad-Brantiite Site, Southeastern Bulgaria

Masanori Kurosawa <sup>1,\*</sup>, Masao Semmoto <sup>2</sup> and Toru Shibata <sup>3</sup><sup>1</sup> Faculty of Life and Environmental Sciences, University of Tsukuba, Tsukuba 305-8572, Japan<sup>2</sup> The Ancient Orient Museum, Tokyo 170-8630, Japan; semmoto@orientmuseum.com<sup>3</sup> Matsudo Museum, Matsudo 270-2252, Japan; s-toru@jcom.zaq.ne.jp

\* Correspondence: kurosawa@geol.tsukuba.ac.jp; Tel.: +81-29-853-6522

**Abstract:** Several pottery sherds from the Svilengrad-Brantiite site, Bulgaria, were mineralogically and petrographically analyzed. The aim was to add information to the very scarce material data available for Early Bronze Age pottery in the southeastern Thrace plain, Bulgaria, in order to examine a possible raw-material source of the pottery. The characterization techniques applied were optical microscopy (OM), petrographic microscopy (PM), scanning electron microscopy coupled with energy dispersive X-ray spectroscopy (SEM-EDS), X-ray fluorescence (XRF) spectroscopy, and X-ray diffraction (XRD). The pottery samples consisted of two typological groups: a local-made type and a cord-impressed decoration type influenced by foreign cultures. All of the samples were produced from fine clay pastes that had a quite similar composition, with abundant mineral grains of similar mineral composition and fragments of metamorphic and granitic rocks. The chemical compositions of each mineral in the grains and fragments were almost identical, and consistent with those from metamorphic and granitic rocks from the Sakar-Strandja Mountains near the study site. The clay paste compositions corresponded to those of illite/smectite mixed-layer clay minerals or mixtures of illite and smectite, and the clay-mineral species were consistent with those in Miocene–Pleistocene or Holocene sediments surrounding the site.

**Keywords:** petrographic analysis; rock fragment; pottery; ceramics; Early Bronze Age; Thrace



**Citation:** Kurosawa, M.; Semmoto, M.; Shibata, T. Mineralogical Characterization of Early Bronze Age Pottery from the Svilengrad-Brantiite Site, Southeastern Bulgaria. *Minerals* **2022**, *12*, 79. <https://doi.org/10.3390/min12010079>

Academic Editors: Daniel Albero Santacreu, José Cristóbal Carvajal López and Adrián Durán Benito

Received: 17 December 2021

Accepted: 5 January 2022

Published: 9 January 2022

**Publisher's Note:** MDPI stays neutral with regard to jurisdictional claims in published maps and institutional affiliations.



**Copyright:** © 2022 by the authors. Licensee MDPI, Basel, Switzerland. This article is an open access article distributed under the terms and conditions of the Creative Commons Attribution (CC BY) license (<https://creativecommons.org/licenses/by/4.0/>).

## 1. Introduction

The Upper Thracian Plain in southern Bulgaria is located between the Balkan Mountains and Rhodope Mountains (Figure 1). The plain underwent social, cultural, and economic transformation in the Early Bronze Age (EBA), from the fourth to the third millennium BCE, as a result of changes in livelihoods, migrations, and the spread of technological innovation. At the beginning of the third millennium BC, the Yamnaya group moved southwards into the plain from the North Pontic area, interacting with the sedentary groups and assimilating into their communities [1,2]. In connection with this issue, the presence of pottery with cord decoration has often been mentioned [2–7]. This pottery style is thought to have spread along with the migration of the Yamnaya groups across the West Pontic region from north to south [2,8], including the possibilities of the movement of potters or the transportation of pottery. This style of pottery, however, has been recovered more frequently from settlement sites other than Yamnaya-style burial mounds (kurgans) in the plain [4,9]; thus, some researchers have argued that indigenous groups in the plain adopted the locally unfamiliar technique of cord-impressed decoration and applied it to pottery [5,7], although the details of this adoption are still a matter of debate.



**Figure 1.** Location map of the Upper Thracian Plain and the Svilengrad-Brantiite site (solid circle) in Bulgaria; geological map of the area around the site (Figure 2) is shown as a dashed box.

Although various cultural and social issues in the plain have been discussed in the context of the typological and stylistic analysis of EBA pottery [10], mineralogical and petrographic analyses have been relatively sparse, except for a few studies of ceramic paste [11,12]. In addition, differences in clay pastes between the foreign-style pottery with cord decoration and local-style pottery have not been clarified. Mineralogical and geochemical analyses of EBA pottery, therefore, are expected to provide insights into the raw materials, provenance, and technology of ceramic manufacture in the area. For these reasons, we analyzed the mineralogical and chemical compositions of mineral grains, rock fragments, and ceramic paste in local- and foreign-style pottery from an EBA site at Svilengrad-Brantiite located in the southeastern part of the Upper Thracian Plain (Figure 1).

## 2. Materials and Methods

### 2.1. Materials

Thirty sherds of EBA pottery (samples SVL01 to SVL30) were selected from the flat settlement at Svilengrad-Brantiite based on their shape and decoration (Table 1). These were fragments of pots, shallow bowls, jars, and jugs. Seven of them (samples SVL24 to SVL30) were decorated with exotic cord impressions, and the remaining 23 (samples SVL01 to SVL23) were indicative of the local EBA2 pottery group. These pottery samples were provided by Dr. Nekhrizov at the National Institute of Archaeology and Museum, Bulgarian Academy of Sciences.

The Svilengrad-Brantiite site is located on a natural levee of the Maritsa River, 2 km southeast of modern Svilengrad, southeastern Bulgaria [13] (Figure 2). At the site, which has an area of approximately 1.5 ha, a series of rescue excavations were conducted between 2004 and 2006 prior to the construction of a railroad, and numerous pits dating to the EBA, Iron Age, medieval era, and Ottoman period were found [13–15]. Many pottery sherds were excavated from the EBA remains together with artifacts commonly found in other settlement sites, such as ground stone, flint tools, clay figurines, and spindle whorls [13–15]. The EBA pottery from the flat settlement at Svilengrad-Brantiite has typological characteristics (shapes and decoration) similar to those of cord-decorated vessels in the Upper Thracian Plain. Thus, the settlement can be dated to the second stage of the EBA (EBA2) in the first half of the third millennium BCE.

**Table 1.** Descriptions of pottery samples studied and mineral grains in the samples. Abbreviations: EBA2—local-made pottery at the second stage of the EBA (EBA2); Cord—pottery with cord decoration; Qtz—quartz; Kfs—potassium feldspar; Mc—microcline (potassium feldspar); Pl—plagioclase; Afs—alkali feldspar; Ms—muscovite; Ep—epidote; Bt—biotite; Opq—opaque minerals; Ttn—titanite; Am—amphibole; Grt—garnet; Chl—chlorite; St—staurolite.

Sample	Type (mm)	Thickness	Surface Color	Internal Color	Mineral Grains		Observed by Optical Microscope										
							Major Species					Minor Species					
							Qtz	Kfs	Mc	Pl	Afs	Ms	Ep	Bt	Opq	Ttn	Am
SVL01	EBA2	8	Dark brown	Dark brown	x	x	x	x	x	x	x	x	x	x	x	x	x
SVL02	EBA2	7	Dark brown	Dark brown	x	x		x	x	x	x	x	x	x	x	x	
SVL03	EBA2	10	Dark brown	Dark brown	x	x	x	x	x	x	x	x	x	x	x		
SVL04	EBA2	6	Dark brown	Dark brown	x	x	x	x	x	x	x	x	x	x	x	x	
SVL05	EBA2	6	Dark brown	Dark brown	x	x	x	x	x	x	x	x	x	x	x		
SVL06	EBA2	7	Dark brown	Dark brown	x	x	x	x	x	x	x	x	x	x	x		
SVL07	EBA2	8	Dark brown	Dark brown	x	x	x	x	x	x	x	x	x	x	x		
SVL08	EBA2	7	Dark brown	Dark brown	x	x	x	x	x	x	x	x	x	x	x		
SVL09	EBA2	7	Dark brown	Dark brown	x	x	x	x	x	x	x	x	x	x	x		
SVL10	EBA2	7	Dark brown	Dark brown	x	x	x	x	x	x	x	x	x	x	x		
SVL11	EBA2	5	Dark brown	Light brown	x	x	x	x	x	x	x	x	x	x	x		
SVL12	EBA2	10	Dark brown	Light brown	x	x	x	x	x	x	x	x	x	x	x		
SVL13	EBA2	12	Dark brown	Light brown	x	x		x	x	x	x	x	x	x	x		
SVL14	EBA2	8	Dark brown	Dark brown	x	x	x	x	x	x	x	x	x	x	x		
SVL15	EBA2	8	Dark brown	Dark brown	x	x	x	x	x	x	x	x	x	x	x		
SVL16	EBA2	6	Dark brown	Dark brown	x	x	x	x	x	x	x	x	x	x	x		
SVL17	EBA2	7	Dark brown	Light brown	x	x	x	x	x	x	x	x	x	x	x		
SVL18	EBA2	7	Dark brown	Dark brown	x	x	x	x	x	x	x	x	x	x	x		
SVL19	EBA2	7	Dark brown	Dark brown	x	x	x	x	x	x	x	x	x	x	x		
SVL20	EBA2	8	Dark brown	Light brown	x	x	x	x	x	x	x	x	x	x	x		
SVL21	EBA2	7	Dark brown	Dark brown	x	x	x	x	x	x	x	x	x	x	x		
SVL22	EBA2	9	Dark brown	Light brown	x	x	x	x	x	x	x	x	x	x	x		
SVL23	EBA2	11	Dark brown	Dark brown	x	x	x	x	x	x	x	x	x	x	x		
SVL24	Cord	8	Dark brown	Light brown	x	x	x	x	x	x	x	x	x	x	x		
SVL25	Cord	10	Dark brown	Light brown	x	x	x	x	x	x	x	x	x	x	x		
SVL26	Cord	8	Dark brown	Light brown	x	x	x	x	x	x	x	x	x	x	x		
SVL27	Cord	10	Dark brown	Light brown	x	x	x	x	x	x	x	x	x	x	x		
SVL28	Cord	8	Dark brown	Light brown	x	x	x	x	x	x	x	x	x	x	x		
SVL29	Cord	9	Dark brown	Light brown	x	x	x		x	x	x	x		x	x		
SVL30	Cord	8	Dark brown	Light brown	x	x	x	x	x	x	x	x	x				

The Svilengrad–Brantiite site is located on the boundary between two different geological bodies: the Sakar–Strandja Mountains to the northwest and northeast side and the Eastern Rhodope massif to the southwest side (Figure 2). These geological bodies are important to consider when determining the major sources of mineral grains, rock fragments, and clay paste in the pottery samples.

The Sakar–Strandja Mountains are mainly composed of Paleozoic basement rocks (mica-schist, gneiss, migmatite, amphibolite, and metagranitoids), Paleozoic granitoids, Mesozoic granitoids, and a cover of Paleozoic to Mesozoic metamorphic rocks [16–20] (Figure 2). The basement rocks and the metamorphic rock cover near the site include muscovite, quartz, plagioclase, microcline, alkali feldspar, biotite, epidote, titanite, bluish-green amphibole, chlorite, opaque minerals, garnet, staurolite, zircon, and apatite [18,21–23]. The basement rocks, granitoids, and metamorphic rocks are overlain by Tertiary sediments (Eocene sedimentary rocks and upper Miocene to partially lowermost Pleistocene sediments [16,18,24,25]). The upper Miocene to Pleistocene sediments underlie and extend a few kilometers around the study site.

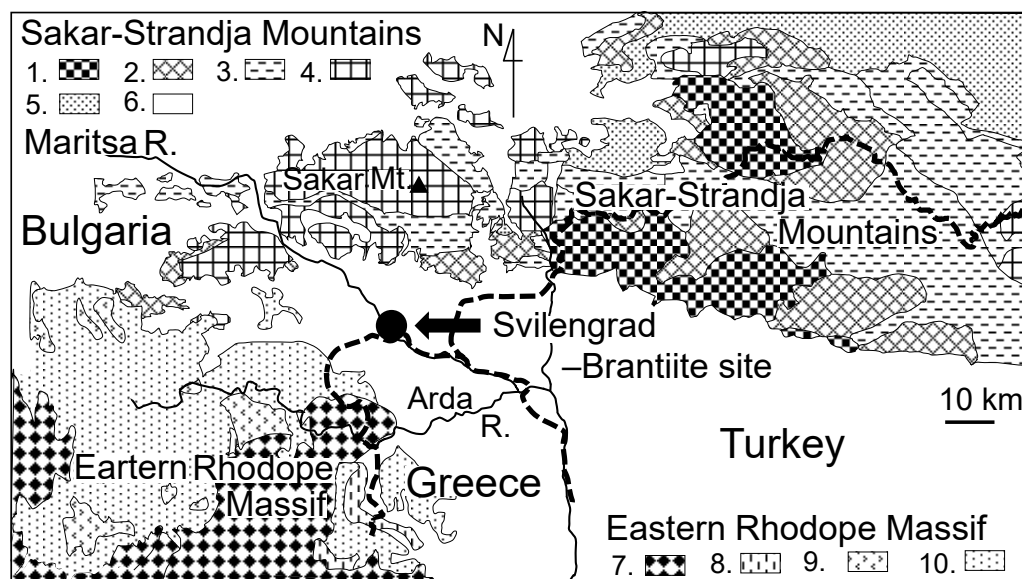


**Figure 2.** Simplified geology of the area around the Svilengrad–Brantiite site (modified after [17,18,26]). Sakar-Strandja Mountains: 1—Paleozoic basement; 2—Paleozoic granitoids; 3—Paleozoic–Mesozoic metamorphic rocks; 4—Mesozoic granitoids; 5—Late Cretaceous sedimentary rocks; 6—Tertiary sediments. Eastern Rhodope Massif: 7—Paleozoic basement; 8—Mesozoic low to medium-grade metamorphic rocks; 9—Tertiary volcanic rocks; 10—Tertiary volcano-sedimentary rocks.

The Eastern Rhodope massif consists mainly of Paleozoic basement rocks (metagranitoids, migmatite, and gneiss), medium- to high-grade metamorphic rocks (amphibolite, eclogite, metabasic rocks, and metaultrabasic rocks), and low-grade metamorphic rocks (greenschist, pelitic schist, phyllite, and marble) [27–30]. These metamorphic rocks include muscovite, quartz, plagioclase, microcline, alkali feldspar, biotite, epidote, titanite, amphibole, chlorite, opaque minerals, garnet, staurolite, and kyanite [27–31]. The basement rocks and metamorphic rocks are surrounded by Cretaceous to Paleogene volcanic and plutonic rocks [28,32,33] and Neogene volcano-sedimentary rocks [34].

The relatively high-grade metamorphic rocks at the Sakar Mountain area are very similar to the basement and metamorphic rocks in the Eastern Rhodope massif [18]. These geological bodies differ, however, in their maximum pressure conditions during metamorphism: ~8 k bar for Sakar Mountain [21,35] and ~13 k bar for the Rhodope massif [27,29,36,37]. Thus, the chemical compositions of their rock-forming minerals may also slightly differ. For this reason, we tried to elucidate the sources of the mineral grains and rock fragments derived from metamorphic rocks by using chemical analysis.

## 2.2. Methods

The pottery samples were cut into slices (approximately 20  $\mu\text{m}$  thick) and doubly polished for microscopic observations under polarized and reflected light. After the observations, the surfaces were coated with a carbon film to prevent electrostatic charging during the analyses with a scanning electron microscope equipped with an energy-dispersive X-ray spectrometer (SEM-EDS). In addition, 1.0 g of the representative samples was powdered for X-ray powder diffraction (XRD) and X-ray fluorescence (XRF) analyses.

Textural observations and chemical analyses of clay pastes and minerals in the samples were performed by using a SEM-EDS (JSM-6010LA, JEOL, Tokyo, Japan) with an accelerating voltage of 20 keV and a beam diameter of approximately 2  $\mu\text{m}$ . Measurement data were quantified by the ZAF method, and the quantified data were further corrected by using standard materials of albite, plagioclase, sanidine, biotite, chlorite, jadeite, Cr-diopside, diopside, rhodonite, kaersutite, almandine, and pyrope (Astimex Standards Ltd., Tronto, Canada). The quantified data were normalized to a total of 100 wt.%.

The major mineral compositions of the pottery samples were determined by using an X-ray diffractometer (MiniFlex600 D/teX Ultra, Rigaku, Tokyo, Japan) with a monochromized Cu K $\alpha$  X-ray (40 kV and 30 mA) and scintillation counter. The 2 $\theta$  scanning angle ranged from 3° to 65°, with 0.02° steps and a scanning speed of 2°/min.

Bulk chemical compositions of the pottery samples were also analyzed by a wavelength dispersive X-ray fluorescence spectrometer (MagiX PW2424, Philips, Eindhoven, Netherlands) using an Rh target X-ray tube operated at 2.4 kW (Paleo Labo Co., Ltd., Japan, Saitama, Japan). Glass-bead samples, fused with a mixture of a powdered specimen and Li<sub>2</sub>B<sub>4</sub>O<sub>7</sub>–LiBO<sub>2</sub> (1:5), were used for XRF analysis. We measured 10 major oxides (Na<sub>2</sub>O, MgO, Al<sub>2</sub>O<sub>3</sub>, SiO<sub>2</sub>, P<sub>2</sub>O<sub>5</sub>, K<sub>2</sub>O, CaO, TiO<sub>2</sub>, MnO, and FeO). The concentrations of these oxides were quantified by a calibration-curve method using 16 standard materials (reference rock powders JA-1, JA-2, JA-3, JB-1, JB-1a, JB-2, JB-3, JF-1, JF-2, JG-1a, JG-2, JG-3, JGb-1, JR-1, JR-2, and JP-1) of the Geological Survey of Japan (National Institute of Advanced Industrial Science and Technology, Tsukuba, Japan).

### 3. Results

#### 3.1. Features of Pottery Samples and Clay Paste

All of the pottery samples were about 7 mm thick (Table 1), and the surfaces were black to brown and were smoothed or burnished (Figure 3a,b). Cross sections of all of the samples were black to reddish-brown, and the samples were produced from fine clay with relatively large amounts of mineral grains and rock fragments (Figure 3c,d). A few elongated voids and rare clay pellets were observed; chaff and other impurities were absent. Minerals grains of muscovite and biotite showed a preferred orientation parallel to the pottery surface (Figure 4a), indicating that the clay paste was kneaded sufficiently during pottery making or possibly that a wheel-made production technique was used [38]. This preferred orientation was also observed for elongated voids in the pottery matrices (Figure 3c). In the SEM observations of the clay pastes in all the samples, the clay minerals showed good adhesion and no partial melting (Figure 4b).

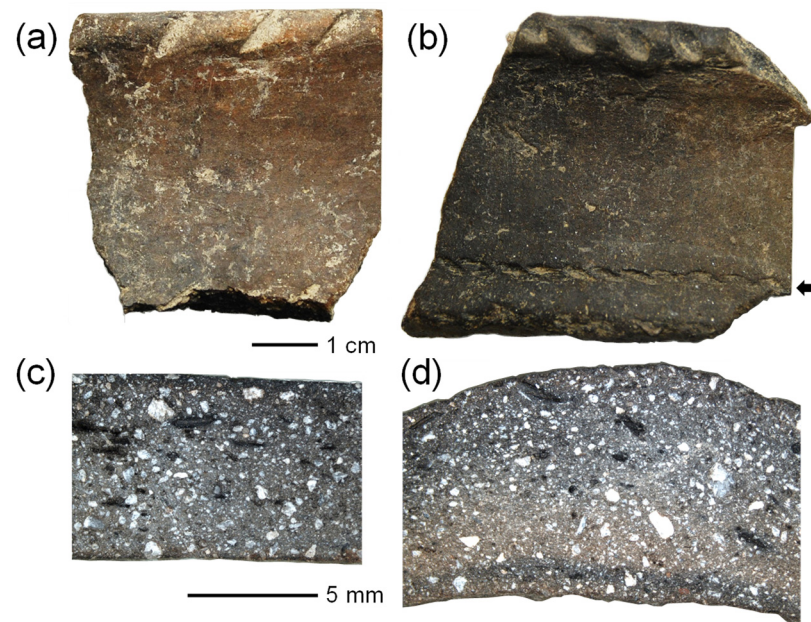


**Figure 3.** (a) Local EBA2 pottery and (b) pottery with cord-impressed decoration (arrow). Scale bars are 1 cm. Cross sections of local EBA2 pottery (c) and pottery with cord-impressed decoration (d). White grains are mineral grains and rock fragments. Black elongated portions are pores. Scale bars are 5 mm.

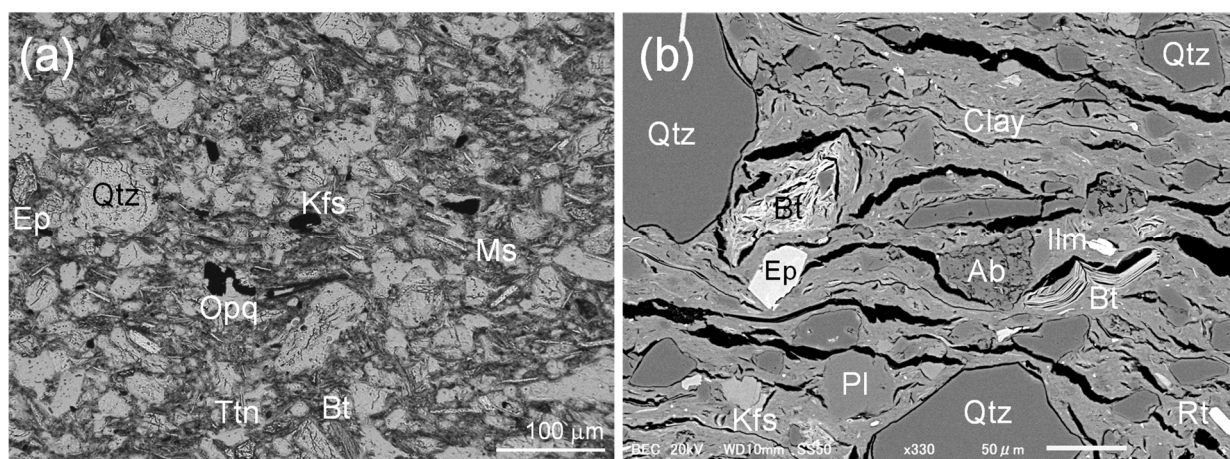


**Figure 4.** (a) Photomicrograph of thin section for pottery sample (SVL24, plane-polarized light). Abbreviations: Qtz—quartz; Ep—epidote; Kfs—potassium feldspar; Ms—muscovite; Opq—opaque mineral (ilmenite); Ttn—titanite; Bt—biotite. (b) SEM image of pottery sample (SVL12). Abbreviations: Ilm—ilmenite; Ab—albite; Pl—plagioclase; Rt—rutile; Clay—clay minerals.

### 3.2. Mineral Grains

The polarized-microscopic observations and SEM-EDS analyses demonstrated that all of the samples included angular to sub-angular grains of dominant quartz, plagioclase, alkali feldspar, potassium feldspar, muscovite, and epidote; subordinate ilmenite, titanite, amphibole, chlorite, biotite, garnet, and staurolite; and trace amounts of zircon, apatite, and rutile. The qualitative volume ratios for the mineral grains were approximately 30 vol.% quartz, 15 vol.% feldspar, 5 vol.% muscovite, less than 1 vol.% other mineral grains and rock fragments, and 50 vol.% clay paste. All of the grains were euhedral in shape or fragmentary. Quartz grains often exhibited wavy extinction. Potassium feldspar and alkali feldspar grains demonstrated a microcline texture and a perthite texture, respectively. Biotite and chlorite were partially altered. Amphiboles were pleochroic and bluish-green and pale green under uncrossed polars.

In the SEM-EDS analyses, most of the plagioclases were found to be rich in sodium (Table 2). Muscovite was relatively enriched in Na and Mg, corresponding to the chemical composition of phengite, which is observed frequently in metamorphic rocks from the Sakar-Strandja Mountains [19,21] and the Eastern Rhodope massif [27,29,31]. Biotite was poor in potassium as a result of alteration (Table 2), and epidote was rich in iron and similar in composition to that from metamorphic rocks [19,29,30] or gabbro [33]. Amphibole exhibited chemical zoning, and its composition corresponded to calcic amphiboles (magnesiohornblende, edenite, ferroedenite, and rare pargasite). Garnet was enriched in iron, corresponding to almandine garnet. Opaque minerals were mostly ilmenite and rarely magnetite. Tiny grains, less than 10 μm in length, of zircon, apatite, and rutile were always observed, but their abundances varied across samples.

The mineral grains in all of the pottery samples showed the same combination of mineral species independent of grain size and grain amount, and the chemical compositions of each mineral were very similar among the samples. The major features of the grains were the similarity of mineral species, relatively large amounts of muscovite and epidote, and a lack of olivine or pyroxene, which are commonly found in igneous rocks. In addition, during the SEM observations, we observed an absence of minerals formed by high-temperature firing and a lack of textures associated with thermal decomposition and partial melting in the mineral grains. These features were identical in both the local EBA2 pottery and the cord-decorated pottery.

**Table 2.** Representative SEM–EDS analyses of minerals from pottery. Abbreviations: (g)—mineral grain; (f)—minerals in rock fragments. \* Numbers of ions in chemical formulae for potassium feldspar and plagioclase were calculated on an 8 oxygen basis, for muscovite and biotite on a 22 oxygen basis, for epidote on a 12.5 oxygen basis, for amphibole on a 23 oxygen basis, and for garnet on a 12 oxygen basis, respectively. Numbers of Fe<sup>3+</sup> in epidote and garnet were calculated based on Fe<sup>2+</sup> or Fe<sup>3+</sup> occupancies in the cation sites and the rest as Fe<sup>3+</sup> or Fe<sup>2+</sup> in the structural formulae. \*\* Numbers of ions in chemical formulae for titanite on a 5 oxygen basis, for staurolite on a 24 oxygen basis, for ilmenite on a 3 oxygen basis, for rutile on a 2 oxygen basis, for zircon and magnetite on a 4 oxygen basis, for apatite on a 26 oxygen basis, and for chlorite (chloritized biotite) on a 28 oxygen basis, respectively.

Potassium Feldspar + A1:R51			Plagioclase		Muscovite		Biotite		Epidote		Amphibole		Garnet							
Wt. %	(g)	(f)	(g)	(f)	(g)	(f)	(g)	(f)	(g)	(f)	(g)	(f)	(g)	(f)						
Na <sub>2</sub> O	0.91	0.74	Na <sub>2</sub> O	9.36	9.42	Na <sub>2</sub> O	0.31	0.25	Na <sub>2</sub> O	0.16	0.15	Na <sub>2</sub> O	0.05	0.04	Na <sub>2</sub> O	2	1.77	Na <sub>2</sub> O	0.05	0.05
MgO	0.01	0.02	MgO	0	0	MgO	2.19	2.19	MgO	9.45	10.39	MgO	0.05	0.07	MgO	9.25	9.42	MgO	3.95	3.58
Al <sub>2</sub> O <sub>3</sub>	18.08	17.92	Al <sub>2</sub> O <sub>3</sub>	22.98	22.71	Al <sub>2</sub> O <sub>3</sub>	31.13	31.02	Al <sub>2</sub> O <sub>3</sub>	16.27	16.98	Al <sub>2</sub> O <sub>3</sub>	29.73	28.28	Al <sub>2</sub> O <sub>3</sub>	12.7	12.24	Al <sub>2</sub> O <sub>3</sub>	20.68	20.72
SiO <sub>2</sub>	65.28	65.31	SiO <sub>2</sub>	62.98	63.32	SiO <sub>2</sub>	49.66	50.68	SiO <sub>2</sub>	40.96	38.2	SiO <sub>2</sub>	39.13	38.92	SiO <sub>2</sub>	44.78	44.75	SiO <sub>2</sub>	37.92	38.34
K <sub>2</sub> O	15.55	15.88	K <sub>2</sub> O	0.03	0.09	K <sub>2</sub> O	11.49	10.87	K <sub>2</sub> O	9.53	9.67	K <sub>2</sub> O	0	0	K <sub>2</sub> O	0.65	0.48	K <sub>2</sub> O	0.05	0.04
CaO	0.06	0	CaO	4.49	4.26	CaO	0.05	0	CaO	0.29	0.18	CaO	23.95	23.85	CaO	10.45	10.68	CaO	3.2	2.99
TiO <sub>2</sub>	0.04	0.12	TiO <sub>2</sub>	0	0.11	TiO <sub>2</sub>	0.57	0.68	TiO <sub>2</sub>	2.5	2.13	TiO <sub>2</sub>	0.26	0.04	TiO <sub>2</sub>	0.56	1.03	TiO <sub>2</sub>	0.03	0
MnO	0	0	MnO	0.03	0	MnO	0	0.04	MnO	0.77	0.69	MnO	0.43	0.37	MnO	0.46	0.27	MnO	4.68	0.92
FeO	0.07	0.01	FeO	0.13	0.08	FeO	4.6	4.26	FeO	20.07	21.61	FeO	6.4	8.43	FeO	19.14	19.35	FeO	29.43	33.35
Total	100	100	Total	100	100	Total	100	99.99	Total	100	100	Total	100	100	Total	99.99	99.99	Total	99.99	99.99
Numbers of ions in chemical formulae *																				
T-site			T-site		T-site		T-site		T-site		T-site		T-site		T-site		T-site		T-site	
Si	3.009	3.014	Si	2.802	2.938	Si	6.51	6.441	Si	5.909	5.657	Si	3.006	3.022	Si	6.577	6.572	Si	3.025	3.055
Al	0.982	0.975	Al	1.184	1.051	Al	1.49	1.559	Al	2.091	2.343	Al1-site			Al	1.423	1.428	Al		
(sum)	3.991	3.989	(sum)	3.986	3.989	(sum)	8	8	(sum)	8	8	Al	2.692	2.589	(sum)	8	8	Al	1.944	1.946
M-site			M-site		M-site		M-site		M-site		M-site		M-site		M-site		M-site		M-site	
Ti	0.001	0.004	Ti	0.004	0.002	Al	3.207	3.399	Al	0.675	0.491	Fe <sup>3+</sup>	0.411	0.547	Al	0.775	0.691	Fe <sup>3+</sup>	0.054	0.054
Fe	0.003	0	Fe	0.003	0.004	Ti	0.065	0.046	Ti	0.271	0.387	(sum)	3.119	3.138	Ti	0.062	0.113	(sum)	2	2
Mn	0	0	Mn	0	0	Fe	0.458	0.425	Fe	2.421	2.999	A2-site			Mg	2.025	2.061	B-site		
Mg	0.001	0.001	Mg	0	0	Mn	0.004	0.001	Mn	0.094	0.047	Fe <sup>2+</sup>	0	0	Fe	2.351	2.377	Fe <sup>2+</sup>	1.91	2.168
K	0.915	0.935	K	0.005	0.004	Mg	0.42	0.209	Mg	2.031	1.616	Mn	0.028	0.025	Mn	0.058	0.034	Mn	0.316	0.062
Na	0.082	0.066	Na	0.808	0.899	(sum)	4.154	4.08	(sum)	5.492	5.54	Mg	0.006	0.008	Ca	1.646	1.681	Mg	0.469	0.426
Ca	0.003	0	Ca	0.202	0.089	A-site			A-site			Na	0.008	0.006	Na	0.084	0.043	Na	0.008	0.008
(sum)	1.005	1.007	(sum)	1.022	0.998	K	1.781	1.812	K	1.753	1.952	Ca	1.971	1.984	(sum)	7.001	7	Ca	0.274	0.255
Total	4.996	4.996	Total	5.009	4.987	Na	0.063	0.098	Na	0.045	0.043	K	0	0	A-site			K	0.005	0.004
						Ca	0	0	Ca	0.045	0	(sum)	2.013	2.023	Na	0.486	0.462	(sum)	2.912	2.923
						(sum)	1.844	1.91	(sum)	1.843	1.995	Total	8.138	8.183	K	0.123	0.09	Total	8.007	7.978
						Total	13.998	13.99	Total	15.335	15.535				(sum)	0.609	0.552			
															Total	15.61	15.552			



### 3.3. Rock Fragments

Rock fragments were angular to sub-angular, 0.1 mm to 2 mm in size, and variable in amount and size. Fifty mineral assemblages were distinguished in the fragments (Table 3). The most abundant rock fragments were polycrystalline quartz with undulatory extinction (Figure 5a), followed by assemblages of quartz + muscovite + epidote or plagioclase + muscovite + epidote with a schistose texture (Figure 5b,c). Metagranitoids and amphibolite with a deformed equigranular texture (Figure 5d,e) and garnet gneiss with a weak banded texture were also observed (Figure 5f).

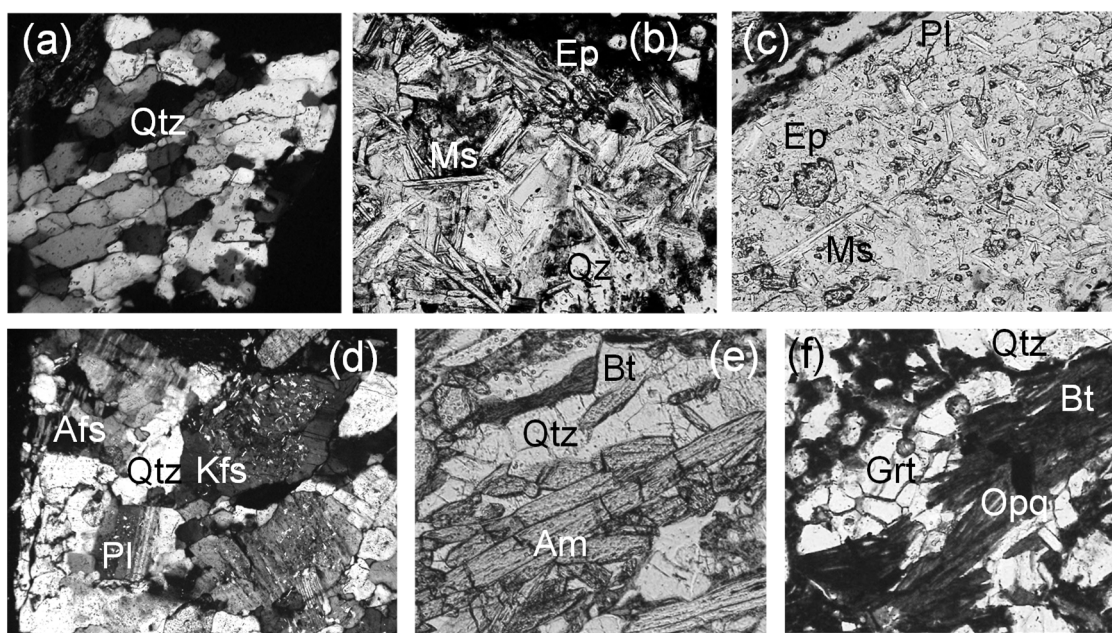


**Figure 5.** Photomicrograph of rock fragments in pottery samples (plane-polarized polar). The vertical sizes are 200  $\mu\text{m}$ . (a) Fragment of quartz aggregate with undulatory extinction. (b) Pelitic or basic schist. (c) Pelitic or basic schist. (d) Metagranitoids or granitic rocks. (e) Basic schist or amphibolite. (f) Garnet gneiss. Abbreviations: Qtz—quartz; Ep—epidote; Ms—muscovite; Pl—plagioclase; Afs—alkali feldspar; Kfs—potassium feldspar; Bt—biotite; Am—amphibole; Grt—garnet; Opq—opaque.

The 50 mineral assemblages could be grouped into five assemblage types on the basis of the mineral species combinations (Table 3). These five mineral assemblage types were estimated to correspond to five kinds of original rock types based on the textures observed in the assemblages: pelitic or basic schist; metagranitoids or granitic rocks; amphibolite or basic schist; pelitic schist; and gneiss (Table 3). Because polycrystalline quartz is always present in these metamorphic rocks, it was considered to have originated from all five rock types. In addition, the chemical compositions of each mineral in the rock fragments were in good agreement with those of the mineral grains in the samples (Table 2), indicating that the mineral grains and rock fragments originated from the same source rocks.

### 3.4. Chemical Composition of Clay Paste

The chemical compositions of the clay pastes without mineral grains or rock fragments were analyzed with SEM-EDS, and average values for five-point analyses were obtained for 10 samples (Table 4).

All of the clay pastes were non-calcareous (<6 wt.% CaO [39]) and possessed relatively lower K<sub>2</sub>O contents than a typical illite [40,41]. The SiO<sub>2</sub> and Al<sub>2</sub>O<sub>3</sub> contents within each sample exhibited a narrow concentration range (Table 4), and the other elements except for CaO and P<sub>2</sub>O<sub>5</sub> showed similar tendencies. These narrow ranges demonstrate that the clay paste had a relatively homogeneous composition within each pottery sample. In addition, the pastes had a very similar oxide concentrations across all samples (Table 4), indicating

that all of the pottery samples had been produced from a clay paste with the same chemical composition. No systematic differences were observed in the chemical content between the local EBA2 group and the cord-decorated group.

**Table 3.** Mineral assemblages observed in rock fragments within pottery and the estimated rock type. Abbreviations: Afs—alkali feldspar; Am—amphibole; Ap—apatite; Bt—biotite; Chl—chlorite; Ep—epidote; Grt—garnet; Ilm—ilmenite; Kfs—potassium feldspar (or microcline); Mus—muscovite; Pl—plagioclase; Qtz—quartz; Rt—rutile; St—staurolite; Ttn—titanite; Zrn—zircon. \* Basic mineral assemblages were estimated based on combinations of the mineral assemblages. Rock types were estimated based on the basic mineral assemblages and textures observed in the assemblages.

Mineral Assemblages	Basic Mineral Assemblages and Estimated Rock Type *
Qtz (polycrystalline with undulatory extinction)	} Various metamorphic rocks
Qtz + Mus, Qtz + Ep	
Qtz + Mus + Ep	} Type (1) Qtz + Ms + Pl + Ep ± Afs ± Chl ± Trv ± Bt ± Ilm ± Aπ : pelitic or basic schist
Qtz + Mus + Ep + Bt	
Pl + Mus, Pl + Ep, Pl + Ilm	
Pl + Mus + Ep, Pl + Mus + Qtz, Pl + Ep + Qtz	
Pl + Ep + Bt	
Pl + Mus + Ep + Ilm	
Qtz + Ep + Afs, Mus + Ep + Afs	
Qtz + Pl + Ep + Afs, Qtz + Mus + Ep + Afs	
Chl + Pl, Chl + Ilm + Afs	
Qtz + Kfs, Qtz + Bt, Qtz + Pl	
Kfs + Mus, Kfs + Bt	
Qtz + Kfs + Mus, Qtz + Kfs + Bt,	
Qtz + Mus + Bt	
Mus + Bt + Ap	
Qtz + Kfs + Mus + Bt	
Qtz + Kfs + Pl + Zrn, Kfs + Pl + Zrn + Ap	
Qtz + Ttn, Pl + Ttn	
Qtz + Mus + Ttn, Pl + Mus + Ttn	
Qtz + Kfs + Mus + Bt + Ttn	
Qtz + Am, Am + Ilm, Am + Ep	} Type (3) : Qtz + Pl + Am + Ilm ± Afs ± Rt ± Zrn : amphibolite or basic schist
Qtz + Ilm, Ilm + Rt, Ilm + Zrn	
Qtz + Pl + Am, Pl + Am + Ilm, Ilm + Rt	} Type (4) : Qtz + Grt + St ± Bt ± Mus ± Ilm ± Rt : pelitic schist
Qtz + Grt + St	
Qtz + Grt + St + Bt + Ilm	} Type (5) : Qtz + Bt + Kfs + Grt: gneiss
Qtz + St + Mus + Ilm + Rt	
Qtz + Bt + Grt, Qtz + Kfs + Grt	

### 3.5. X-ray Fluorescence (XRF)

The bulk chemical composition of six pottery samples was analyzed by XRF. The oxide contents were very similar among the samples, and no systematic differences were observed between the pottery types (Table 4). The results for two major compounds, SiO<sub>2</sub> and Al<sub>2</sub>O<sub>3</sub>, agreed within approximately 7% among the samples (Table 4), but the values were higher than the corresponding SEM-EDS values of the clay pastes without mineral grains or rock fragments. The higher SiO<sub>2</sub> and Al<sub>2</sub>O<sub>3</sub> contents were thought to result from the contributions of quartz and feldspar as mineral grains and rock fragments. The average values for each compound were within one standard deviation of those estimated for an average mixture of clay paste and mineral grains (Table 4). The clay paste and the mineral grain values in the average mixture were selected from Tables 2 and 4, respectively. The mixture ratio was assumed to be 47.6 vol.% clay paste, 25.7 vol.% quartz grains, 16.4 vol.% plagioclase grains, 5.0 vol.% potassium feldspar grains, 4.2 vol.% muscovite grains, 0.8 vol.% ilmenite grains, and 0.3 vol.% apatite grains. The volume ratios of the major minerals were very close to those of the mineral grains observed with the optical microscope.

**Table 4.** Chemical compositions of clay pastes in pottery samples, bulk pottery samples, mixtures of clay paste and mineral grains, and Maritsa River sediments. <sup>\*1</sup> Average value of the five-point analyses; standard deviations in parentheses. <sup>\*2</sup> Pottery type: EBA2—local-made type; Cord—pottery with cord decoration. <sup>\*3</sup> Average values for the results of 10 pottery samples; standard deviations in parentheses. <sup>\*4</sup> Average values for the results of six pottery samples and standard deviations. <sup>\*5</sup> Mixture composition estimated from the average clay paste composition and the chemical compositions of the mineral grains (Table 1). The mixing ratios were 47.6 vol.% clay paste, 25.7 vol.% quartz, 16.4 vol.% plagioclase, 5.0 vol.% potassium feldspar, 4.2 vol.% muscovite, 0.8 vol.% ilmenite, and 0.3 vol.% apatite. <sup>\*6</sup> Average composition excluding water content of low-calcareous-content alluvial (flood-plain) sediments near the Maritsa River [42]; standard deviations in parentheses. –, Not analyzed.

Clay Paste Compositions (wt.% <sup>*1</sup> ) Determined by SEM-EDS Analyses (without Mineral Grains or Rock Fragments)											
Sample	SVL01	SVL03	SVL04	SVL11	SVL12	SVL18	SVL23	SVL24	SVL25	SVL30	Average <sup>*3</sup>
Type <sup>*2</sup>	EBA2	Cord	Cord	Cord							
Na <sub>2</sub> O	0.37 (0.08)	0.34 (0.15)	0.35 (0.06)	0.43 (0.21)	0.37 (0.16)	0.41 (0.15)	0.41 (0.10)	0.30 (0.05)	0.46 (0.18)	0.31 (0.12)	0.38 (0.04)
MgO	2.51 (0.18)	2.75 (0.19)	2.55 (0.25)	2.48 (0.36)	2.06 (0.48)	3.26 (0.46)	2.34 (0.57)	3.03 (0.80)	2.50 (0.43)	2.63 (0.45)	2.61 (0.32)
Al <sub>2</sub> O <sub>3</sub>	24.66 (1.35)	20.09 (1.39)	23.53 (0.84)	22.28 (1.56)	23.39 (1.86)	23.77 (1.68)	27.35 (1.35)	20.95 (2.13)	26.43 (0.84)	23.69 (0.75)	23.61 (2.11)
SiO <sub>2</sub>	56.91 (1.45)	58.34 (2.29)	58.29 (1.45)	58.17 (1.43)	57.93 (2.48)	57.76 (1.44)	55.25 (1.24)	59.11 (2.97)	56.10 (1.21)	55.81 (1.20)	57.37 (1.18)
P <sub>2</sub> O <sub>5</sub>	0.47 (0.18)	1.77 (0.52)	0.73 (0.11)	2.52 (0.42)	1.90 (0.47)	0.12 (0.06)	0.31 (0.09)	1.35 (0.17)	0.23 (0.14)	0.94 (0.56)	1.03 (0.71)
K <sub>2</sub> O	3.61 (0.34)	3.58 (0.69)	3.11 (0.52)	2.74 (0.53)	2.77 (0.43)	2.87 (0.55)	2.64 (0.51)	3.45 (0.96)	2.10 (0.18)	3.07 (0.26)	2.99 (0.46)
CaO	2.43 (0.42)	3.35 (1.20)	1.96 (0.16)	2.74 (0.47)	3.18 (0.61)	1.47 (0.22)	1.36 (0.52)	2.42 (0.32)	1.65 (0.69)	2.27 (0.95)	2.28 (0.65)
TiO <sub>2</sub>	0.73 (0.38)	0.68 (0.08)	0.66 (0.10)	0.71 (0.19)	0.66 (0.19)	0.73 (0.12)	0.72 (0.12)	0.57 (0.10)	0.69 (0.15)	0.99 (0.21)	0.71 (0.14)
MnO	0.04 (0.05)	0.03 (0.03)	0.03 (0.03)	0.04 (0.03)	0.05 (0.11)	0.05 (0.02)	0.08 (0.11)	0.01 (0.02)	0.03 (0.05)	0.04 (0.07)	0.04 (0.02)
FeO	8.27 (2.31)	9.07 (0.56)	8.79 (0.99)	7.89 (0.91)	7.68 (0.92)	9.56 (1.03)	9.54 (0.62)	8.81 (0.75)	9.81 (1.10)	10.25 (1.15)	8.97 (0.91)
Total	100.00	100.00	100.00	100.00	99.99	100.00	100.00	100.00	100.00	100.00	99.99
Bulk compositions (wt.%) of pottery samples obtained by XRF analyses								Mixture of clay and mineral grains <sup>*5</sup>		Maritsa River sediments <sup>*6</sup>	
Sample Type	SVL01 EBA2	SVL04 EBA2	SVL11 EBA2	SVL12 EBA2	SVL24 Cord	SVL25 Cord	Average <sup>*4</sup>	Average clay paste composition + content of several mineral grains		Low-calcareous-content alluvial sediments (average)	
Na <sub>2</sub> O	1.51	1.9	1.7	1.6	2.22	1.6	1.76 (0.26)	1.77		1.65 (0.19)	
MgO	0.94	1.58	1.22	0.92	1.69	1.04	1.23 (0.33)	1.33		1.82 (0.45)	
Al <sub>2</sub> O <sub>3</sub>	14.88	18.2	16.12	15.86	16.52	16.1	16.28 (1.09)	17.22		16.63 (0.00)	
SiO <sub>2</sub>	72.37	63.54	68.09	70.56	66.73	71.62	68.82 (3.35)	68.69		69.2 (0.83)	
P <sub>2</sub> O <sub>5</sub>	0.22	0.88	1.24	0.7	0.48	0.12	0.6 (0.42)	0.62		–	
K <sub>2</sub> O	3.04	3.09	2.57	2.68	2.85	2.58	2.8 (0.23)	2.69		2.29 (0.01)	
CaO	1.68	2.56	2.32	1.82	2.5	1.35	2.04 (0.49)	1.99		1.56 (0.05)	
TiO <sub>2</sub>	0.54	1.02	0.76	0.63	0.95	0.65	0.76 (0.19)	0.78		0.72 (0.01)	
MnO	0.06	0.07	0.11	0.06	0.09	0.06	0.08 (0.02)	0.08		0.1 (0.01)	
FeO	3.79	5.63	4.59	4.32	5.01	4.27	4.6 (0.65)	4.81		5.01 (0.21)	
Total	99.03	98.48	98.71	99.15	99.04	99.38	98.97	99.98		98.98	

In addition, the average XRF values agreed within one standard deviation with those of alluvial flood-plain sediments near the Maritsa River [42] (Table 4). The alluvial sediments include clay, mineral grains, and pebbles or gravel [42,43], as well as pebbles of metamorphic rocks [44]. Mineral grains in the sediments consist mainly of quartz, plagioclase, potassium feldspar, and muscovite; trace amounts of amphibole, epidote, titanite, zircon, opaque minerals; and variable amounts of calcite [42–44]. Calcite was not present in some layers of the sediments [42,43], and an assemblage of mineral grains excluding calcite was in good agreement with that of the mineral grains in the pottery samples. Therefore, the average chemical composition of the alluvial sediments in Table 4 was estimated based on the analytical data of low-calcareous sediments [42], excluding water contents.

### 3.6. X-ray Diffraction (XRD)

In six representative samples, major diffraction peaks of muscovite, quartz, and sodium-rich plagioclase (albite) were observed (Figure 6). Diffraction peaks of clay minerals and high-temperature firing minerals such as mullite were absent. The peak intensities of muscovite relative to those of other minerals were strongly lower in some samples, although the abundance of muscovite in the mineral grains was nearly constant in the clay pastes in the microscopic observations. Thus, the attenuation of the peak intensity in muscovite is thought to have originated from the deterioration of its crystal structure as a result of thermal alteration. A very weak peak of chlorite was also observed in one sample. Because chlorite was observed microscopically in many samples, the rare detection of a chlorite peak may also be the result of thermal decomposition.

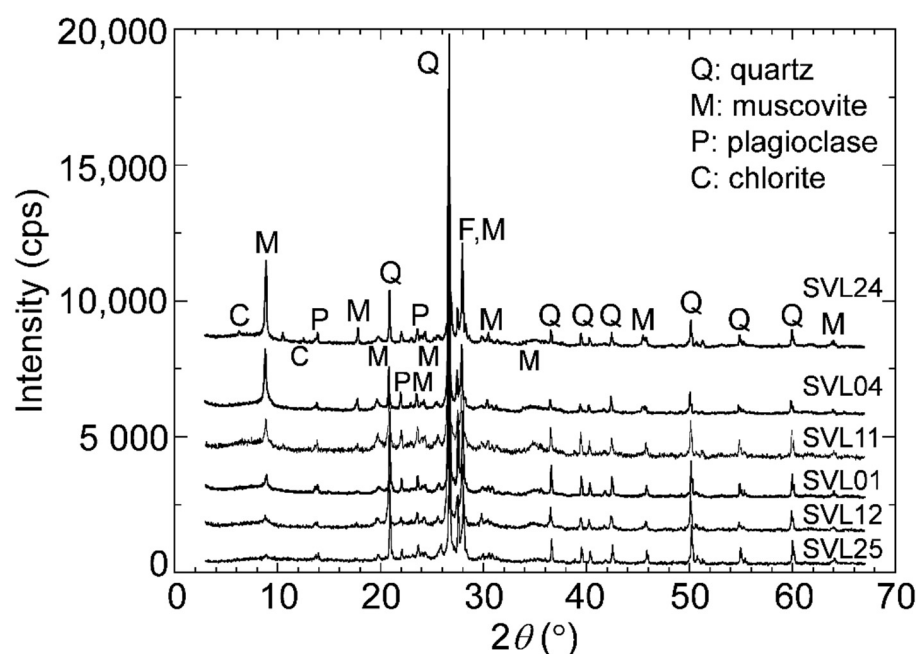


Figure 6. XRD patterns of pottery samples (SVL01, SVL04, SVL11, SVL12, SVL24, and SVL25).

## 4. Discussion

### 4.1. Origin and Source of the Mineral Grains and Rock Fragments

Both the rock fragments and the mineral grains in the pottery samples were inferred to have originated from metamorphic and metagranitoid or granitic rocks. Such metamorphic and granitic rocks are distributed widely in both the Sakar–Strandja Mountains and the Eastern Rhodope massif. Therefore, we examined the source area of the fragments and grains by comparing the mineral chemistry of the grains, fragments, and rocks in both areas using data from previous publications.

The atomic ratios of Ti/Fe in muscovite from metamorphic and granitic rocks exhibited different trends for the Sakar–Strandja Mountains and the Eastern Rhodope massif

(Figure 7a), and the majority of mineral grains and rock fragments plotted within the Sakar–Strandja region. The Ca/Fe atomic ratios in amphibole in the rocks also had different trends in the Sakar–Strandja and Rhodope areas (Figure 7b) and the grains and fragments plotted within the Sakar–Strandja region. These trends show that the mineral grains and rock fragments in the pottery originated from metamorphic and granitic rocks in the Sakar–Strandja Mountains. A similar trend was also observed in a Fe + Mg vs. Al plot for staurolite (not shown). These kinds of differences in correlations among elements, however, were unclear for plagioclase, alkali-feldspar, epidote, and garnet.

Upper Miocene to Pleistocene sediments (Ahmatovo Formation) are widely distributed from the southern slope of the Sakar–Strandja Mountains to the area surrounding the site [16]. The Ahmatovo Formation is also exposed within a few kilometers of the site; northwest of the site, it includes pebbles and gravel (up to boulder size) derived from metamorphic and granitic rocks of the Sakar–Strandja Mountains [24]. Typical raw-material sampling distances are thought to be within approximately 7 km of a given site [45], so the raw materials of the grains and fragments were probably derived from the Ahmatovo Formation. The alluvial sediments near the Maritsa River are also a possible raw-material source because sand grains occur in the same mineral assemblage as the pottery mineral grains and metamorphic rocks are present as pebbles [42–44]. Because the pottery mineral grains and rock fragments were angular to sub-angular, sub-angular sand grains and non-abraded pebbles in the sediments may have been the source material.

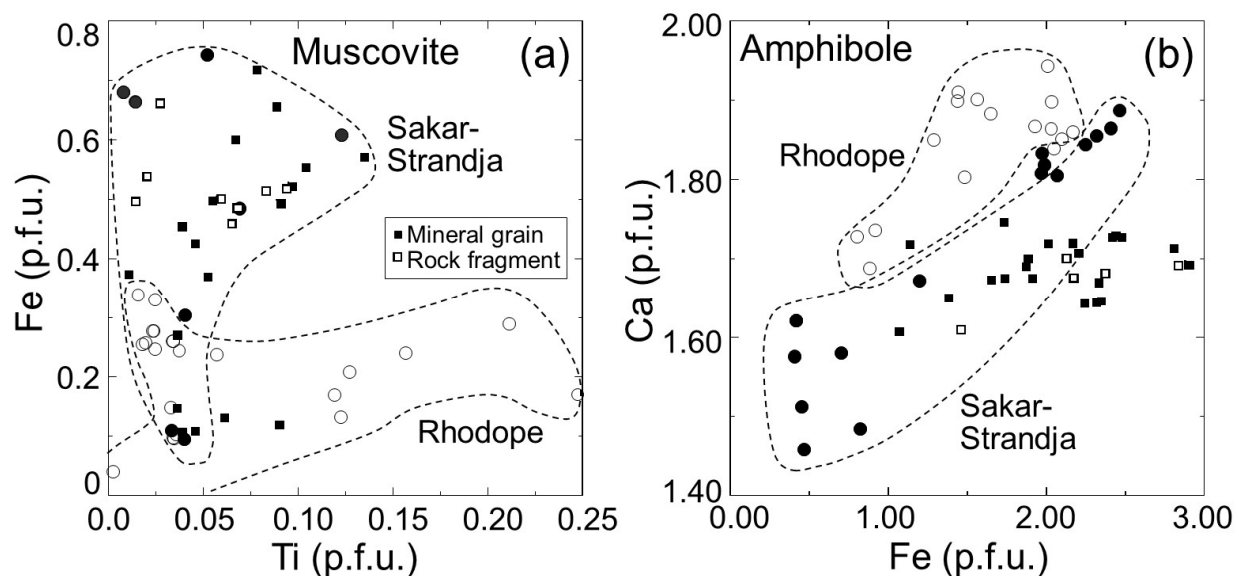


**Figure 7.** (a,b) Correlations of cations per formula unit (pfu) of minerals in mineral grains and rock fragments from pottery samples and metamorphic and igneous rocks from the Eastern Rhodope massif and Sakar–Strandja Mountains. (a) Ti vs. Fe in muscovite. Open circles, muscovite in gneiss and pelitic schists from the Eastern Rhodope massif [27,29,31]; solid circles, muscovite in gneiss and pelitic schists from the Sakar–Strandja Mountains [19,21]; closed squares, muscovite as mineral grains; solid squares, muscovite in rock fragments. (b) Fe vs. Ca in amphibole. Open circles, amphibole in schist, amphibolite, metamorphosed gabbro, and gabbro from the Eastern Rhodope massif [29,30,33,36]; solid circles, amphibole in amphibolite, metagranitoids, and gabbro from the Sakar–Strandja Mountains [19,46]; closed squares, amphibole as mineral grains; solid square, amphibole in rock fragments.

#### 4.2. Chemical Features of the Clay Paste

The chemical features of the clay pastes were examined by using oxide correlation plots based on the chemical compositions of representative clay minerals (kaolinite, illite, smectite, and illite/smectite mixed-layer clay minerals [41]) and the SEM-EDS results for the clay pastes without mineral grains or rock fragments (Table 4). In the  $\text{SiO}_2$  vs.  $\text{Al}_2\text{O}_3$

diagram (Figure 8a), the clay paste data were plotted in the compositional region between representative illite and smectite or representative illite/smectite mixed-layer clay minerals. In the  $\text{Na}_2\text{O} + \text{K}_2\text{O}$  vs.  $\text{CaO}$  diagram (Figure 8b), the clay pastes also fell within the region of the representative illite/smectite mixed-layer clay minerals, although some clay pastes demonstrated an excess of  $\text{CaO}$  content outside the range of the mixed-layer clay minerals. The excess  $\text{CaO}$  may have resulted from the presence of nano-sized fragments of calcite dispersed in the clay pastes. The compositions of the clay pastes are basically thought to correspond to those of illite/smectite mixed-layer clay minerals or a mixture of smectite and illite.

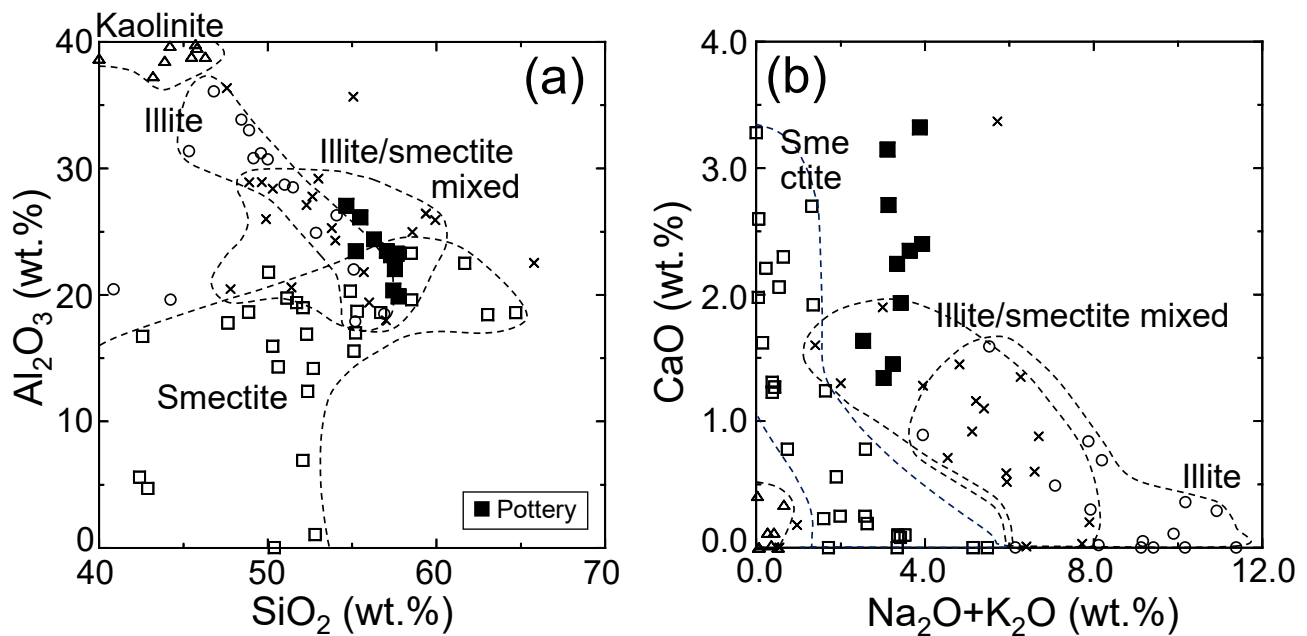


**Figure 8.** (a,b) Correlations of oxide contents in pottery clay pastes and representative clay minerals (kaolinite, illite, smectite, and illite/smectite mixed-layer clay minerals). Solid squares, clay paste from pottery samples; open triangles, kaolinite [41]; open circles, illite [41]; open squares, smectite [41]; crosses, illite/smectite mixed-layer clay minerals [41]. (a)  $\text{SiO}_2$  vs.  $\text{Al}_2\text{O}_3$  and (b)  $\text{Na}_2\text{O} + \text{K}_2\text{O}$  vs.  $\text{CaO}$ .

Illite/smectite mixed-layer clay minerals are often formed by the chemical weathering of basic schist [41,47]. On the eastern slope of the Sakar Mountain, mixed-layered illite/smectite and kaolinite were found to be the predominant clay minerals in clay from Miocene sediments corresponding to the Ahmatovo Formation [48]. Illite and smectite have also been identified in the clay sediments [48]. In addition, Holocene fluvial sediments from the Maritsa River consist mainly of clayey–silty sediments, sands, and gravels. Smectite is the principal clay mineral in the clayey–silty sediments (about 77%); illite (13%) and kaolinite (10%) are subordinate [43]. Thus, the outcrop area of the Ahmatovo Formation (i.e., the flood plains of the Maritsa River) was most likely the collecting site for the raw clay materials.

#### 4.3. Estimated Firing Temperature

Melting textures for the clay pastes and feldspar grains were not identified in the SEM observations. The starting points of melting for clay minerals are approximately 750–800 °C under reduced conditions and approximately 800–850 °C under oxidized conditions [39]; thus, the pottery samples were considered to have been fired at temperatures of less than 800 °C.

Some pottery samples demonstrated a marked decrease in the diffraction intensities of muscovite and chlorite (Figure 2), regarded as indicative of thermal decomposition

during pottery firing. The diffraction peak of muscovite in a clay matrix disappears at a temperature over 850 °C [49–51], and a decrease in the diffraction intensities is clearly observed at a temperature range of 700–800 °C [52]. Chlorite in a clay matrix is completely decomposed at a temperature of 750 °C under reduced or oxidized conditions [53,54]. Taking these factors into account, the firing temperature of the pottery is thought to have been 700–800 °C, which is close to the values of 750–850 °C reported for EBA pottery in northwestern Thrace, Bulgaria [55]. In addition, the existence of dark cores in the present samples indicates a firing of short duration or in an incomplete state of oxidation. Such firing conditions may be a feature of EBA pottery in the Thrace plain.

#### 4.4. Relationship between Petrographic and Typological Features of Pottery

The studied pottery samples contained chemically homogeneous clay pastes with rare clay pellets and without impurities. We presume that levigation was performed during the preparation of the clay raw materials. As a mixture of well-sorted clays and abundant angular mineral grains and rock fragments is exceptional in a naturally deposited clay bed, the mineral grains and rock fragments in the pottery samples are interpreted as artificially tempered materials introduced after the levigation step. The presence of artificially tempered materials in the samples appears to be consistent with the large volume ratios of tempered minerals and fragments observed under the microscope. Large volume ratios of mineral grains were also estimated in the calculations of the mixture compositions of clay paste and mineral grains (Table 4). The preferred orientation of muscovite grains and elongated voids in the clay pastes indicated that a high-skill technique was used during pottery making.

The techniques for pottery making, mineral species of the grains, rock types of the fragments, and chemical compositions of clay pastes were nearly the same in both the local EBA2 group pottery and the cord-decorated pottery. These results indicate that both pottery types were produced from the same raw materials and using the same production techniques. Thus, the cord-decorated pottery samples were probably local pottery made under the influence of a foreign culture.

## 5. Conclusions

The EBA pottery samples from the Svilengrad-Brantiite site in southeastern Bulgaria exhibited dark-colored surfaces and orange to reddish-brown cross sections with a dark core. The pottery was produced from non-calcareous clay pastes with abundant mineral grains and fragments of metamorphic and granitic rocks, was created using high-skill techniques, and was fired at moderate temperatures (700–800 °C). The two typological groups, local-made EBA2 and cord-decorated types, were quite similar in terms of mineral grains, rock fragments, clay pastes, and production techniques; thus, both types of pottery from Svilengrad-Brantiite are considered to be of the local style, most probably made by the inhabitants.

The mineral grains and rock fragments were inferred to have originated from metamorphic and granitic rocks in the Sakar-Strandja Mountains. Because fragments and separated grains of these rocks are present as gravel, pebbles, and sand in Neogene sediments and Maritsa River sediments, they were most likely collected from an area near the site. The clay materials were also likely to have been procured from river sediments or Tertiary sediments on the slopes of the Sakar-Strandja Mountains. The procurement of the raw materials near the site and the high-skill techniques used to make the pottery may be characteristic of EBA pottery from the southeastern part of the Upper Thracian Plain.

**Author Contributions:** Conceptualization, M.K. and M.S.; methodology, M.K. and T.S.; software, M.K.; validation, M.K. and M.S.; formal analysis, M.K. and T.S.; investigation, M.K., M.S. and T.S.; resources, M.K. and M.S.; data curation, M.K. and T.S.; writing—original draft preparation, M.K. and M.S.; writing—review and editing, M.K.; visualization, M.K.; supervision, M.K. and M.S.; project administration, M.K. and M.S.; funding acquisition, M.K. and M.S. All authors have read and agreed to the published version of the manuscript.

**Funding:** This study was supported in part by the Japan Society for the Promotion of Science Grants-in-Aid for Scientific Research (no. 18H05447 to M.K. and 19K13399 to M.S.).

**Data Availability Statement:** The dataset is presented directly in the present study. Additional data (unpublished) are available upon request from the corresponding author (M.K.).

**Acknowledgments:** The authors wish to thank G. Nekhrizov of the National Institute of Archaeology and Museum, Bulgarian Academy of Sciences, for provision of the pottery samples; K. Matsumoto of Tokai University, Japan, for sample preparation; and H. Takehara of Paleo Labo Co., Ltd., Japan, for conducting the XRF analyses. The authors would also like to thank the two anonymous reviewers for their useful comments that helped in the revision of this manuscript.

**Conflicts of Interest:** The authors declare no conflict of interest.

## References

1. RAnthony, D.W. *The Horse, the Wheel, and Language: How Bronze-Age Riders from the Eurasian Steppes Shapes the Modern World*; Princeton University Press: Princeton, NJ, USA, 2007.
2. Heyd, V. Yamnaya Groups and Tumuli west of the Black Sea. In *Ancestral Landscape. Burial Mounds in the Copper and Bronze Ages (Central and Eastern Europe–Balkans–Adriatic–Aegean, 4th–2nd millennium B.C.)*; Borgna, E., Müller-Celka, S., Eds.; Travaux de la Maison de l’Orient, TMO 58; Maison Orient: Lyon, France, 2011; pp. 535–555.
3. Georgiev, G. Beiträge zur Erforschung des Neolithikums und der Bronzezeit in Südbulgarien. *Arch. Austr.* **1967**, *42*, 90–144.
4. Roman, P.; Dodd-Oprîtescu, A.; János, P.; Hauptmann, H.; Schrickel, W. *Beiträge zur Problematik der Schnurverzierten Keramik Südosteuropas*; P. von Zabern: Mainz am Rhein, Germany, 1992.
5. Nikolova, L. Data about sea contacts during the Early Bronze Age in south-eastern Europe (c. 3500/3400–2350/2250 B.C.). *Thracia Pontica* **1994**, *5*, 57–86.
6. Lichardus, J.; Lichardus-Itten, M. Nordpontische Beziehungen während der frühen Vorgeschichte Bulgariens. *Thracia* **1995**, *11*, 31–62.
7. Leshtakov, K.; Tsirtsoni, Z. Caesurae in the Bronze Age chronology of Eastern Bulgaria. In *Der Schwarzmeerraum vom Neolithikum bis in Die Früheisenzeit (6000–600 v. Chr.). Kulturelle Interferenzen in der Zirkumpontischen Zone und Kontakte mit Ihren Nachbargebieten*; Nikolov, V., Schier, W., Eds.; Verlag Marie Leidorf GmH: Rahden, Germany, 2016; pp. 477–491.
8. Harrison, R.J.; Heyd, V. The transformation of Europe in the third millennium BC: The example of ‘Le Petit Chasseur I+III’ (Sion, Valais, Switzerland). *Praehist. Z* **2007**, *82*, 129–214. [[CrossRef](#)]
9. Semmoto, M. Chronology and Regional Interaction on Pottery in Early Bronze Age, Bulgaria: Focusing on Material Analysis of Tell Dyadovo. Ph.D. Thesis, Tokai University, Kanagawa, Japan, 2015.
10. Leshtakov, K. Troy and upper Thrace: What happened in the EBA 3? (Interrelations Based on Pottery Evidence). In *Early Bronze Age Troy: Chronology, Cultural Developments and Interregional Contacts*; Pernicka, E., Ünlüsoy, S., Blum, S., Eds.; Verlag Dr. Rudolf Habelt: Bonn, Germany, 2016; pp. 239–255.
11. Semmoto, M.; Kannari, T.; Shibata, T.; Leshtakov, K. Petrographic and Chemical characterization of Early Bronze Age pottery from Sokol Himitliyata in Nova Zagora Region: An interim report. *Stud. Archaeol. Univ. Serdicensis Diss. Ser.* **2018**, *6*, 153–167.
12. Leshtakov, K.; Machev, P.; Popova, T.; Vangelov, D.; Vangelova, V.; Stoilkova, T.; Petrova, V.; Ilieva, D.; Nikolova, N.; Chavdarova, S.; et al. Social dimensions of technology of ceramic production in southeast Bulgaria in 6th–2nd mill. BC. *Interdiscip. Stud.* **2019**, *26*, 33–106.
13. Nekhrizov, G.; Tzvetkova, J. Iron Age ritual pits near Svilengrad. In *Spasitelni Arheologicheski Razkopki po Traseto na Zhelezopatnata Liniya Plovdiv–Svilengrad Prez 2005 [Rescue Excavations along the Route of the Plovdiv–Svilengrad Railway in 2005]*; Nikolov, V., Nekhrizov, G., Tzvetkova, J., Eds.; Faber: Veliko Tarnovo, Bulgaria, 2008; pp. 331–493.
14. Nekhrizov, G. Iron Age pit sanctuary and Early Bronze Age settlement near the town of Svilengrad. In *Spasitelni Arheologicheski Razkopki po Traseto na Zhelezopatnata Liniya Plovdiv–Svilengrad Prez 2004 [Rescue Excavations along the Route of the Plovdiv–Svilengrad Railway in 2004]*; Nikolov, V., Nekhrizov, G., Tzvetkova, J., Eds.; Faber: Veliko Tarnovo, Bulgaria, 2006; pp. 397–548.
15. Valentinova, M.; Nenova, D. Early Bronze Age site near Svilengrad. In *Spasitelni Arheologicheski Razkopki po Traseto na Zhelezopatnata Liniya Plovdiv–Svilengrad Prez 2005 [Rescue Excavations along the Route of the Plovdiv–Svilengrad Railway in 2005]*; Nikolov, V., Nekhrizov, G., Tzvetkova, J., Eds.; Faber: Veliko Tarnovo, Bulgaria, 2008; pp. 494–526.
16. Kozhoukharov, D.; Boyanov, I.; Kozhoukharova, E.; Goranov, A.; Savov, S.; Shilyafov, G. *Explanatory Note to the Geological Map of Bulgaria on Scale 1:100000, Svilengrad Map Sheet*; Geology and Geophysics Corporation: Sofia, Bulgaria, 1995.
17. Okay, A.; Satır, M.; Tüysüz, O.; Akyüz, S.; Chen, F. The tectonics of the Strandja Massif: Late-Variscan and mid-Mesozoic deformation and metamorphism in the northern Aegean. *Int. J. Earth Sci.* **2001**, *90*, 217–233. [[CrossRef](#)]
18. Gerdjikov, I. Alpine metamorphism and granitoid magmatism in the Strandja Zone: New data from the Sakar Unit, SE Bulgaria. *Turkish J. Earth Sci.* **2005**, *14*, 167–183.
19. Sunal, G.; Satır, M.; Natal’in, B.A.; Topuz, G.; Vonderschmidt, O. Metamorphism and diachronous cooling in a contractional orogen: The Strandja Massif, NW Turkey. *Geol. Mag.* **2011**, *148*, 580–596. [[CrossRef](#)]
20. Marchev, P.; Ganev, V.; Klain, L. New LA-ICP-MS U-Pb zircon dating for Strandja granitoids (SE Bulgaria): Evidence for two-stage late Variscan magmatism in the internal Balkanides. *Turkish J. Earth Sci.* **2015**, *24*, 230–248. [[CrossRef](#)]

21. Tzankova, N. Chemical characterization of garnets and P-T conditions of metamorphism of the Triassic rocks occurring to the south of Oreschnik, South-East Bulgaria. *Ann. Univ. Min. Geol. St. Ivan Rilski* **2005**, *48*, 155–160.
22. Tzankova, N.; Petrov, O. ICP AES, microprobe, and X-ray powder diffraction data for garnets from metamorphic rocks in the Sakar region, SE Bulgaria. *Geochem. Mineral. Petrol. Sofia* **2006**, *44*, 73–89.
23. Kamenov, B.K.; Vergilov, V.; Dabovski, C.; Vergilov, I.; Ivchinova, L. The Sakar batholith–petrology, geochemistry and magmatic evolution. *Geochem. Mineral. Petrol. Sofia* **2010**, *48*, 1–37.
24. Schaller, M.; Lachner, J.; Christl, M.; Maden, C.; Spassov, N.; Ilg, A.; Böhme, M. Authigenic Be as a tool to date river terrace sediments?—An example from a Late Miocene hominid locality in Bulgaria. *Quat. Geochronol.* **2015**, *29*, 6–15.
25. Ivanov, D.; Lazarova, M. Past climate and vegetation in Southeast Bulgaria—A study based on the late Miocene pollen record from the Tundzha Basin. *J. Palaeogeogr.* **2019**, *8*, 3. [[CrossRef](#)]
26. Caracciolo, L.; Orlando, A.; Critelli, S.; Kolios, N.; Manetti, P.; Marchev, P. The Tertiary Trace Basin of SE Bulgaria and NE Greece: A review of petrological and mineralogical data of sedimentary sequences. *Acta Vulcanol.* **2015**, *25*, 21–41.
27. Mposkos, E.; Liati, A. Metamorphic evolution of metapelites in the high-pressure terrane of the Rhodope zone, northern Greece. *Can. Mineral.* **1993**, *31*, 401–424. [[CrossRef](#)]
28. Marchev, P.; Raicheva, R.; Downes, H.; Vaselli, O.; Chiaradia, M.; Moritz, R. Compositional diversity of Eocene–Oligocene basaltic magmatism in the Eastern Rhodopes, SE Bulgaria: Implications for genesis and tectonic setting. *Tectonophysics* **2004**, *393*, 301–328. [[CrossRef](#)]
29. Nagel, T.J.; Schmidt, S.; Janák, M.; Froitzheim, N.; Jahn-Awe, S.; Georgiev, N. The exposed base of a collapsing wedge: The Nestos Shear Zone (Rhodope metamorphic province, Greece). *Tectonics* **2011**, *30*, TC4009. [[CrossRef](#)]
30. Bonev, N.; Ovtcharova-Schaltegger, M.; Moritz, M.R.; Marchev, P.; Ulianov, A. Peri-Gondwanan Ordovician crustal fragments in the high-grade basement of the Eastern Rhodope Massif, Bulgaria: Evidence from U-Pb LA-ICP-MS zircon geochronology and geochemistry. *Geodin. Acta* **2013**, *26*, 207–229. [[CrossRef](#)]
31. Mposkos, E. High-pressure metamorphism in gneisses and pelitic schists in the East Rhodope Zone (N. Greece). *Mineral. Petrol.* **1989**, *41*, 25–39. [[CrossRef](#)]
32. Yanev, Y.; Ivanova, R. Mineral chemistry of the collision-related acid Paleogene volcanic rocks of the Eastern Rhodopes, Bulgaria. *Geochem. Mineral. Petrol. Sofia* **2010**, *48*, 39–65.
33. Raicheva, R.; Marchev, P.; Georgiev, S.; Ichev, M. Geochemistry, mineral composition and conditions of crystallization of accessory-rich gabbro associated with adakitic rocks of the Drangovo pluton, Rhodope Massif. *C. R. Acad. Bulg. Sci.* **2018**, *71*, 220–229.
34. Caracciolo, L.; Orlando, A.; Marchev, P.; Critelli, S.; Manetti, P.; Raycheva, R.; Riley, D. Provenance of Tertiary volcanoclastic sediment in NW Thrace (Bulgaria): Evidence from detrital amphibole and pyroxene geochemistry. *Sediment. Geol.* **2016**, *336*, 120–137. [[CrossRef](#)]
35. Chavdarova, S.; Machev, P. Amphibolites from Sakar Mountain—geological position and petrological features. In Proceedings of the Bulgarian Geological Society, National Conference with International Participation “Geosciences 2017”, Sofia, Bulgaria, 7–8 November 2017; pp. 49–50.
36. Raeva, E.; Cherneva, Z. Metamorphic grade of the Madan unit in the southern part of the Central Rhodopes, Bulgaria. *Geochem. Mineral. Petrol. Sofia* **2009**, *47*, 135–161.
37. Moulas, E.; Schenker, F.L.; Burg, J.P.; Kostopoulos, D. Metamorphic conditions and structural evolution of the Kesebir-Kardamos dome: Rhodope metamorphic complex (Greece-Bulgaria). *Int. J. Earth Sci.* **2017**, *106*, 2667–2685. [[CrossRef](#)]
38. Braekmans, D.; Degryse, P. Petrography: Optical microscopy. In *The Oxford Handbook of Archaeological Ceramic Analysis*; Hunt, A.M.W., Ed.; Oxford University Press: Oxford, UK, 2016; pp. 233–265.
39. Maniatis, Y.; Tite, M.S. Technological Examination of Neolithic-Bronze Age pottery from central and southeast Europe and from the Near East. *J. Archeol. Sci.* **1981**, *8*, 59–76. [[CrossRef](#)]
40. Ionescu, C.; Hoeck, V.; Ghergari, L. Electron microprobe analysis of ancient ceramics: A case study from Romania. *Appl. Clay Sci.* **2011**, *53*, 466–475. [[CrossRef](#)]
41. Wilson, M.J. *Sheet Silicates: Clay Minerals, Rock-Forming Minerals*; The Geological Society of London: London, UK, 2013; Volume 3C.
42. Yaneva, M. Comperative sedimentologic characteristics of young sediments (Pliocene–Holocen) disturbed by Chirpan Fault. *Rev. Bulgarian Geol. Soc.* **2006**, *67*, 41–49.
43. Yaneva, M.; Lazarova, M. Preliminary sedimentological and palynological studies of Quaternary deposits from paleoseismological trench “Cherna Gora”, Chirpan district. *C. R. Acad. Bulg. Sci.* **2004**, *57*, 71–76.
44. Yaneva, M.; Todorova, N.; Katsarov, G.; Petrova, V.; Bacvarov, K. By the rivers of Nova Nadezhda: Dynamics of human–environment interaction at a prehistoric site in Upper Thrace. *Geol. Balc.* **2017**, *46*, 65–72.
45. Arnold, D. *Ceramic Theory and Cultural Process*; Cambridge University Press: Cambridge, UK, 1985.
46. Pristavova, S.; Tzankova, N.; Gospodinov, N.; Filipov, P. Petrological study of metasomatic altered granitoids from Kanarata deposit, Sakar Mountain, southeastern Bulgaria. *J. Mining Geol. Sci.* **2019**, *62*, 53–61.
47. Chamley, H. *Clay Sedimentation*; Springer: Berlin/Heidelberg, Germany, 1989.
48. Ilieva, A.; Milakovska, Z. Mineral composition of the clay fractions from sediments of Troianovo-North mine, East Maritza Basin (Bulgaria). In Proceedings of the Annual Scientific Conference of the Bulgarian Geological Society, GEOSCIENCES 2007, Sofia, Bulgaria, 13–14 November 2017; pp. 39–41.

49. Riccardi, M.P.; Messiga, B.; Duminuco, P. An approach to the dynamics of clay firing. *Appl. Clay Sci.* **1999**, *15*, 393–409. [[CrossRef](#)]
50. Hajjaji, M.; Kacim, S.; Boulmane, M. Mineralogy and firing characteristics of a clay from the valley of Ourika (Morocco). *Appl. Clay Sci.* **2002**, *21*, 203–212. [[CrossRef](#)]
51. Papadopouloul, D.N.; Lalia-Kantouri, M.; Kantiranis, N.; Stratis, J.A. Thermal and mineralogical contribution to the ancient ceramics and natural clays characterization. *J. Therm. Anal. Calorim.* **2006**, *84*, 39–45. [[CrossRef](#)]
52. Ortega, L.A.; Zuluaga, M.C.; Alonso-Olazabal, A.; Murelaga, X.; Alday, A. Petrographic and geochemical evidence for long-standing supply of raw materials in Neolithic pottery (Mendandia site, Spain). *Archaeometry* **2010**, *52*, 987–1001. [[CrossRef](#)]
53. Maniatis, Y.; Simopoulos, A.; Kostikas, A.; Perdikatsis, V. Effect of reducing atmosphere on minerals and iron oxides developed in fired clays: The role of Ca. *J. Am. Ceram. Soc.* **1983**, *66*, 773–781. [[CrossRef](#)]
54. Maggetti, M.; Neururer, C.; Ramseyer, D. Temperature evolution inside a pot during experimental surface (bonfire) firing. *Appl. Clay Sci.* **2011**, *53*, 500–508. [[CrossRef](#)]
55. Kostadinova-Avramova, M.; Jordanova, N.; Jordanova, D.; Grigorov, V.; Lesigyarski, D.; Dimitrov, P.; Bozhinova, E. Firing temperatures of ceramics from Bulgaria determined by rock-magnetic studies. *J. Archeol. Sci. Rep.* **2018**, *17*, 617–633. [[CrossRef](#)]